
Climate Data Record (CDR) Program

Climate Algorithm Theoretical Basis Document (C-ATBD)

Fundamental Climate Data Record (FCDR) for Special Sensor Microwave/Imager (SSM/I)



CDR Program Document Number: CDRP-TMP-0006
Originator Document Number: TBD
Version 1.0 / June 1, 2013

RESPONSIBILITY

Prepared By: Wesley Berg Project Lead Colorado State Univ.

Signature

Date

Reviewed By: Christian Kummerow Principal Investigator Colorado State Univ.

Signature

Date

Reviewed By: <Name> <Title> <Organization>

Signature

Date

Approved By: <Name> <Title> <Organization>

Signature

Date

Approved By: <Name> <Title> <Organization>

Signature

Date

REVISION HISTORY

Version/ Revision	Author	Description	Revised Sections	Date
V01R00	Wesley Berg Colorado State Univ.	Initial submission to CDR Program	New Document	06/25/2013

TABLE of CONTENTS

1. INTRODUCTION	6
1.1 Purpose	6
1.2 Definitions.....	6
1.3 Document Maintenance.....	6
2. OBSERVING SYSTEMS OVERVIEW.....	6
2.1 Products Generated	6
2.2 Instrument Characteristics.....	6
3. ALGORITHM DESCRIPTION.....	8
3.1 Algorithm Overview	8
3.2 Processing Outline	8
3.2.1 Read Input.....	10
3.2.2 Calculate Ephemeris	10
3.2.3 Calculate Geolocation	10
3.2.4 Quality Control.....	12
3.2.5 Cross-track Bias Correction.....	13
3.2.6 Ta to Tb Conversion	14
3.2.7 Intercalibration	14
3.2.8 RADCAL Correction	16
3.2.9 Write Output	17
3.3 Algorithm Input	18
3.3.1 Primary Sensor Data	18
3.3.2 Ancillary Data (optional)	18
3.3.3 Derived Data.....	18
3.3.4 Forward Models.....	18
3.4 Theoretical Description.....	19
3.4.1 Physical and Mathematical Description	19
3.4.2 Data Merging Strategy.....	20
3.4.3 Numerical Strategy	20
3.4.4 Calculations	20
3.4.5 Look-Up Table Description	20
3.4.6 Parameterization	22
3.4.7 Algorithm Output.....	22
4. TEST DATASETS AND OUTPUTS	23
4.1 Test Input Datasets	23
4.2 Test Output Analysis	23
4.2.1 Reproducibility	23
4.2.2 Precision and Accuracy	23
4.2.3 Error Budget	23
5. PRACTICAL CONSIDERATIONS.....	23
5.1 Numerical Computation Considerations	23
5.2 Programming and Procedural Considerations.....	24
5.3 Quality Assessment and Diagnostics	24

5.4	Exception Handling.....	24
5.4.1	Conditions Checked	24
5.4.2	Conditions Not Checked.....	25
5.4.3	Conditions Not Considered Exceptions	25
5.5	Algorithm Validation.....	25
5.5.1	Validation during Development.....	25
5.6	Processing Environment and Resources	27
6.	ASSUMPTIONS AND LIMITATIONS.....	29
6.1	Algorithm Performance.....	29
6.2	Sensor Performance.....	29
7.	FUTURE ENHANCEMENTS.....	29
7.1.1	Cross-track bias corrections	29
7.1.2	Warm scene intercalibration	29
7.1.3	Solar and lunar intrusions.....	29
8.	REFERENCES	30

LIST of FIGURES

Search Word online help for “Add or delete captions” for assistance with this table

Figure 1: SSM/I Scan Configuration.....	7
Figure 2: FCDR for SSM/I Outline Processing Flowchart.	9
Figure 3: Diagram showing (a) the local zenith (up), east and west vectors on Earth’s surface relative to the GCI frame; and (b) the zenith and azimuth angles relative to the pointing vector D.	11
Figure 4: Diagram of angles associated with the solar beta angle.....	12
Figure 5: Plots of intercalibration estimates from each implementation by channel for F13 F14.....	15
Figure 6: Timeseries of original observed Tb22v (blue) and the RADCAL-corrected Tb22v (purple) based on Equation 3 for ocean scenes between 80S and 80N. The corresponding hot load temperature (dashed red line) is also shown with moderate dips in the hot load temp indicated by the light gray shaded regions and large dips indicated by the dark gray shaded regions. The black vertical line in August of 2006 indicates when the RADCAL beacons were activated.	17
Figure 7: Time series of a) total precipitable water, b) ocean surface wind speed, and c) cloud liquid water path based on the SSM/I FCDR.....	27

LIST of TABLES

Search Word online help for “Add or delete captions” for assistance with this table

Table 1: SSM/I channel characteristics	8
Table 2: Error Budget.....	23
Table 3: Processing Environment.....	28

ACRONYMS AND ABBREVIATIONS

Acronym or Abbreviation	Meaning
APC	Antenna Pattern Correction
CATBD	Climate Algorithm Theoretical Basis Document
CDR	Climate Data Record
DMSP	Defense Meteorological Satellite Program
FCDR	Fundamental Climate Data Record
FNMOC	Fleet Numerical Meteorology and Oceanography Center
NCDC	National Climatic Data Center
NOAA	National Oceanic and Atmospheric Administration
NRL	Naval Research Laboratory
SDR	Sensor Data Record (contains TB data)
SGP4	Simplified General Perturbations orbital model
SSM/I	Special Sensor Microwave/Imager
SSMIS	Special Sensor Microwave Imager/Sounder
TA	Antenna Temperature
TB	Brightness Temperature
TDR	Temperature Data Record (contains TA data)
TLE	Two Line Element

1. Introduction

1.1 Purpose

The purpose of this document is to describe the algorithm used to create the Colorado State University (CSU) Fundamental Climate Data Record (FCDR) of brightness temperature data from the series of six Special Sensor Microwave/Imager (SSM/I) instruments on board the Defense Meteorological Satellite Program (DMSP) spacecraft F08, F10, F11, F13, F14 and F15. The actual algorithm is defined by the computer program (code) that accompanies this document, and thus the intent here is to provide a guide to understanding that algorithm, from both a scientific perspective and in order to assist a software engineer performing an evaluation of the code.

1.2 Definitions

None currently.

1.3 Document Maintenance

Synchronization between this document and the algorithm is achieved through version and revision numbers. The version and revision numbers found on the front cover of this document can be compared with the values of `VERSION` and `REVISION` in the source file `params.h`. If the document applies to the algorithm, then these numbers will match. If they don't match and it is found that the document needs to be updated, then the header comment in the file `ssmi_fcdr.c` should be consulted – under its `HISTORY` section is a description of the changes for each version and revision from which the necessary updates to this document can be made.

2. Observing Systems Overview

2.1 Products Generated

The data product generated by this algorithm is the Fundamental Climate Data Record (FCDR) of brightness temperature (Tb) data from the SSM/I sensors, including five low-resolution channels (Tb19v, Tb19h, Tb22v, Tb37v, Tb37h) and two high-resolution channels (Tb85v, Tb85h), stored in netCDF version 4.0 files that include the necessary metadata and supplementary data fields. The data fields are described in detail section 3.4.7 below.

2.2 Instrument Characteristics

Data supplied to this algorithm was collected by SSM/I instruments on board the DMSP satellites F08, F10, F11, F13, F14 and F15. The DMSP series satellites are in sun-synchronous polar orbits at an altitude of approximately 830 km. The instrument is a seven channel linearly polarized passive microwave radiometer operating at

frequencies of 19.35, 22.235, 37.0 (low-resolution), and 85.5 (high-resolution) GHz. The 19.35, 37.0, and 85.5 GHz frequencies have dual-polarization (vertical and horizontal), and the 22.235 GHz frequency has only vertical polarization. The instrument scans through 102 degrees for each scanning revolution producing a swath approximately 1400 km wide. The A-scan data is recorded for all channels, while the B-scan data is only recorded for the high resolution channels. This configuration is shown in Figure 1. Detailed specifications for the spacecraft and instrument are given by Hollinger et al. (1987) and Hollinger (1989, 1991).

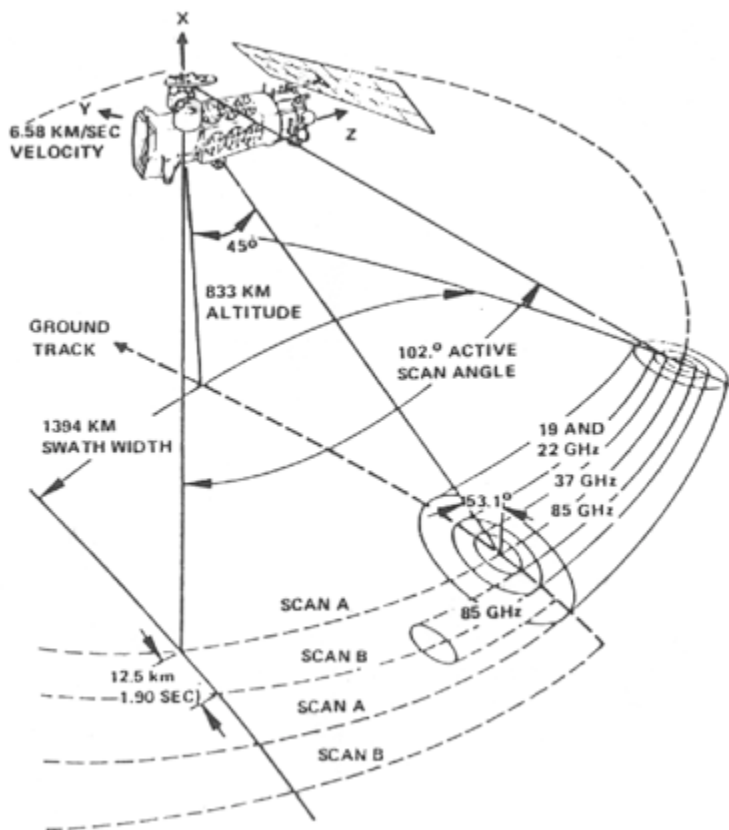


Figure 1: SSM/I Scan Configuration.

SSM/I channel characteristics:

Center Frequencies (GHz)	19.35	19.35	22.235	37.0	37.0	85.5	85.5
Polarization	V	H	V	V	H	V	H
Bandwidth (MHz)	250	250	250	1000	1000	1500	1500
Sensitivity (K)	0.6	0.6	0.6	0.6	0.6	1.1	1.1
EFOV (km along track x km across track)	69 x 43	69 x 43	50 x 40	37 x 28	37 x 29	15 x 13	15 x 13
Sampling Interval (km along track x km across track)	25 x 25	12.5 x 12.5	12.5 x 12.5				
Integration Time (msec)	7.95	7.95	7.95	7.95	7.95	3.89	3.89

Main Beam Efficiency (%)	96.1	96.5	95.5	91.4	94.0	93.2	91.1
Beamwidth (half-power, degrees)	1.87	1.87	1.65	1.10	1.10	0.43	0.45

Table 1: SSM/I channel characteristics

Channel characteristics shown above are from:

- Hollinger et al. (1987), Table 2.1 (EFOV, Beamwidth), Section 2.2 (Sampling Interval), and Table 2.2 (Beam Efficiency).
- Raytheon (2000), Table 3-1 (Integration Time).

3. Algorithm Description

3.1 Algorithm Overview

The algorithm operates on input BASE files, which contain the original antenna temperature (Ta) and calibration data for seven channels as input, processes the data through a number of stages, and creates output FCDR files of brightness temperature (Tb) for the seven channels. The processing stages include: calculate spacecraft ephemeris; calculate pixel geolocation; quality control; cross-track bias correction; convert antenna temperatures to brightness temperatures via an antenna pattern correction; intercalibrate to get physically a consistent Tb record across the different satellites; and correct the Tb22v channel of F15 after RADCAL activation in August of 2006 for Tb contamination.

3.2 Processing Outline

The steps of this algorithm include reading the input data, seven sequential processing stages each of which can be turned on or off with a flag in the code, and writing the output data file. Each stage is described in this section. The processing flow is shown in Figure 2.

FCDR for SSM/I Processing Flowchart

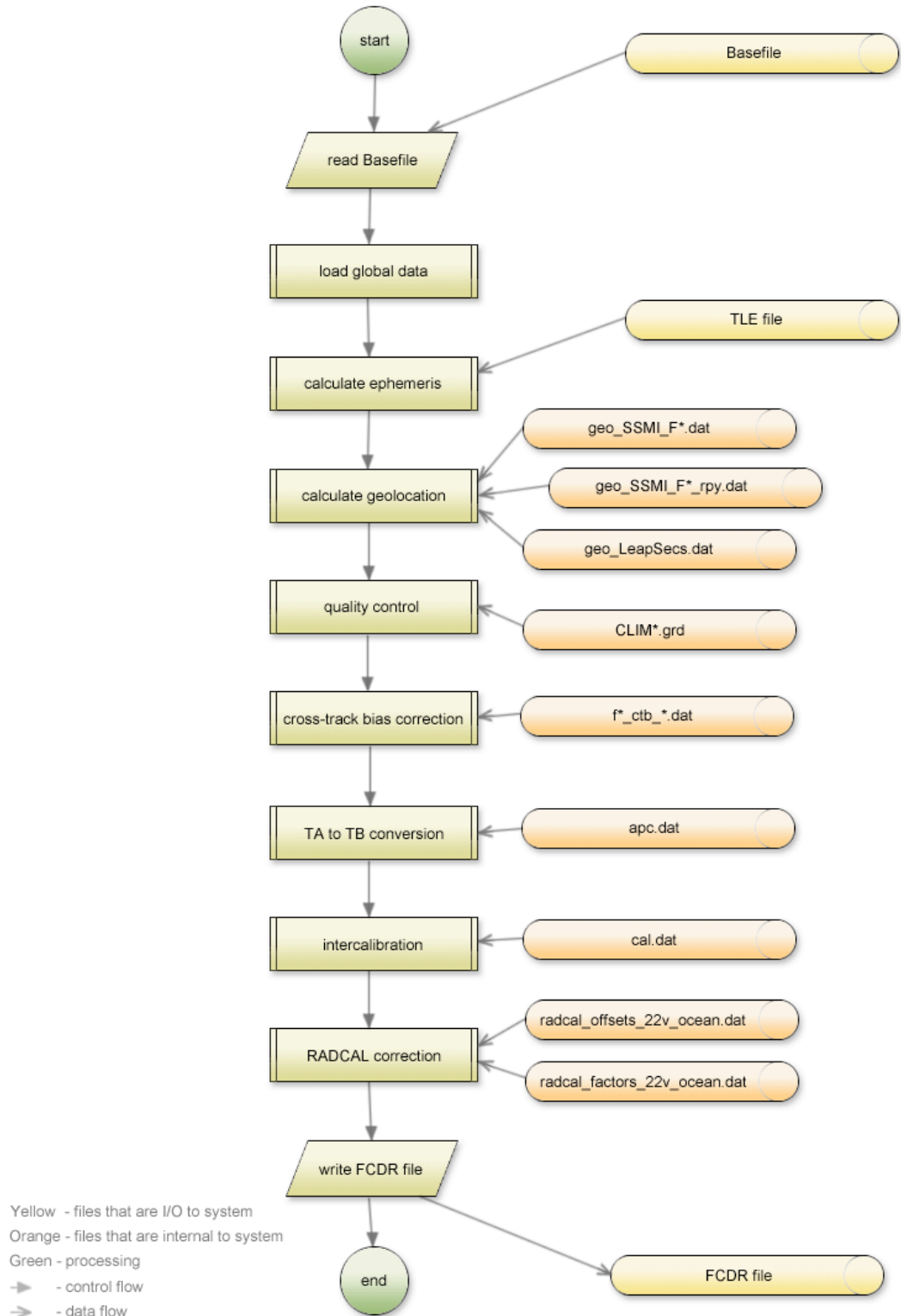


Figure 2: FCDR for SSM/I Outline Processing Flowchart.

3.2.1 Read Input

Data from the input BASE file (see section 3.3.3), optional two-line element (TLE) files (see section 3.3.2), and look-up tables (see section 3.4.5), is read and stored in global variables that are accessed by the subsequent steps. Space is allocated to store output data and certain fields are prepopulated from the input data.

3.2.2 Calculate Ephemeris

The spacecraft position and velocity have been precomputed from TLE orbital elements files and are stored in the input BASE files. Because the TLE files are not generally publicly available and cannot be publicly distributed at this time, the algorithm currently uses the precomputed spacecraft position and velocity data stored in the input BASE files. The Simplified General Perturbations (SGP4) code used to compute the spacecraft position and velocity from the TLE files, however, is included as part of the FCDR algorithm package. Given available TLE files the option to recompute the spacecraft ephemeris is available within the code. For the initial FCDR processing this option was turned off and the position and velocity information stored in the BASE files was used. When this processing stage is turned on, a flag additionally allows a choice between recomputing the ephemeris from the TLE when the time of the TLE is closer than that used in the BASE file or regardless of timing.

3.2.3 Calculate Geolocation

Taking as input the spacecraft position and velocity along with sensor mount angle data and spacecraft orientation data, the geolocation or latitude and longitude of each pixel is calculated and stored. Additional information related to the spacecraft view angles and associated sun angles are also computed. These include the satellite zenith and azimuth angles and solar zenith and azimuth angles, which provide the direction of the satellite and the sun from the normal to the Earth for each pixel. The satellite zenith angle is also referred to as the Earth incidence angle (EIA), which is extremely important for retrieval algorithms as it affects the resulting Tb. The sun glint angle is also computed and provided to identify potential specular reflection from the sun over water surfaces that may also impact retrieval algorithms. Additional information computed at this stage includes angles relating the position of the sun relative to the spacecraft direction of motion, whether or not the spacecraft is in the Earth's shadow, and the time since the spacecraft entered into the Earth's shadow or time since eclipse. Only the EIA and sun glint angles are written out in the FCDR files, but the other angles/fields are computed for analysis purposes. Monthly estimates of the spacecraft attitude, or roll, pitch, and yaw angles, were estimated based on a coastline analysis, which is described in detail by Berg et al. (2013). The geolocation calculation is described in detail in a CSU technical report by Sapiano et al. (2010). The following values are calculated:

3.2.3.1 Pixel Geolocation (Geodetic Latitude and Longitude)

The process for calculating the pixel latitude and longitude starts with the calculation of the Instantaneous Field-Of-View (IFOV) matrix in sensor coordinates. Several rotations are required to obtain the IFOV in Geocentric Inertial (GCI) coordinates. First there is the sensor-to-spacecraft rotation that obtains the IFOV relative to the spacecraft. Next there is the spacecraft-to-orbital (geodetic nadir pointing) rotation that obtains the IFOV relative to the path of the spacecraft. Finally, there is the orbital-to-GCI rotation that obtains the IFOV in GCI coordinates. With the IFOV in GCI coordinates, the intersection of the IFOV with the oblate spheroid used to model Earth is calculated and this is then used to get geocentric, then geodetic latitude and longitude.

3.2.3.2 Satellite Zenith and Azimuth

In order to calculate the satellite zenith (i.e. Earth Incidence Angle or EIA) and azimuth angles, it is necessary to first determine the local zenith (up), north and east vectors. The satellite zenith angle is the angle between the local up vector and the pointing vector and the azimuth angle is the angle between the projection of the pointing vector on the surface and the local north vector where positive azimuth angle is clockwise when viewed from above.

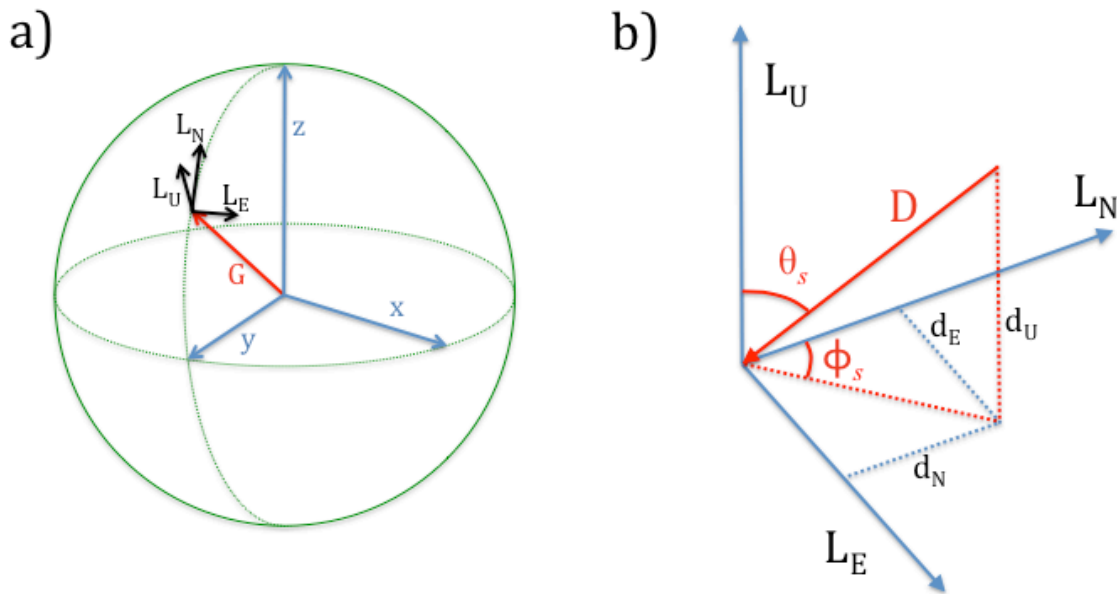


Figure 3: Diagram showing (a) the local zenith (up), east and west vectors on Earth's surface relative to the GCI frame; and (b) the zenith and azimuth angles relative to the pointing vector \mathbf{D} .

3.2.3.3 Solar Angles

Various solar angles are calculated based on the Sun position vector in GCI coordinates determined as described in Appendix C, section C4 of Sapiro et al. (2010). Solar beta angle, sun glint angle, and solar zenith and azimuth angles are found using the Sun

position vector. The time since eclipse is also calculated to provide information on solar heating of the spacecraft based on how long it has been in sunlight or shadow.

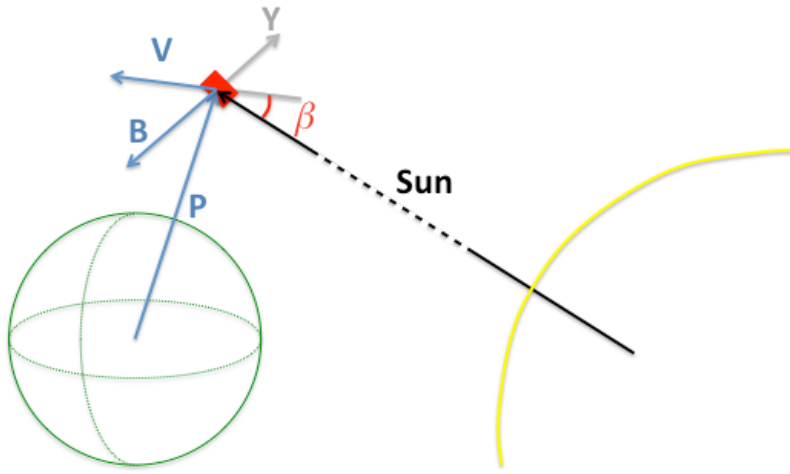


Figure 4: Diagram of angles associated with the solar beta angle.

3.2.4 Quality Control

The quality control processing stage (*qual_control.c*) consists of multiple procedures, which check for potentially erroneous data, correct it if possible, and set the corresponding quality flag. Note that the quality control is done on the input *Ta* prior to the application of the antenna pattern correction (APC). The quality flag values are specified in the file metadata and are defined in the include file *quality_flags.h*. There is a quality flag value for each scan and pixel, with one flag for the low-resolution channels, and one for the high-resolution channels. The flag values consist of three categories with a value of zero indicating good data, values between 1 and 99 indicating a warning or caution, and values from 100 and above indicating an error. For pixels with flag values ≥ 100 the affected *Tb* are subsequently set to missing. The warning flags provide the user information on potential issues, which are often algorithm dependent. For example, a quality flag value of 1 indicates possible sun glint, which is only an issue over reflective surfaces like water and is not an issue at all for some retrievals. A short description of the various quality control procedures follows.

3.2.4.1 Correct *Ta*

Erroneous spikes in hot and cold loads are identified. For affected data, count values are reconstructed from antenna temperatures, the hot and cold load values are interpolated from neighboring scans, corrected antenna temperatures are then computed, and the quality flag is set to indicate that this *Ta* correction has been applied. This correction is described in detail in Berg and Rodriguez-Alvarez (2012).

3.2.4.2 Check BASE file

Some quality control checks were done during the creation of the BASE files including checks for erroneous pixel geolocation and/or large variance from climatology for multiple data scans. This routine sets the associated FCDR quality flag and sets the affected output Tb to missing.

3.2.4.3 Check Geolocation

For data where the original pixel location, given by latitude and longitude, is more than 100 kilometers away from the computed location, the Ta data are set to missing and a quality flag set to indicate a geolocation issue.

3.2.4.4 Check Sensor

Data is set to missing and the quality flag is set for known sensor issues as determined from documented issues and data monitoring. For example, dates corresponding to the failure of first the 85v and then the 85h channels on the F08 SSM/I were determined from an analysis of the data and hardcoded into this routine. The details of which satellites and orbits/dates have known sensor issues are hard-coded into the function that performs this check rather than read from a file.

3.2.4.5 Check Climatology

For each channel, scans where a significant fraction of pixels differ from the climatological mean values (determined as described in section 3.4.5.2) by more than 3 standard deviations are flagged. Two levels of climatology checks are identified. A climatology warning flag is set for scans near the threshold (within 5%) and the Ta data are retained. For scans exceeding this threshold, an error flag value is set in the corresponding quality flag and the Ta data is set to missing.

3.2.4.6 Check Pixel

Pixels where the distance between adjacent pixels along a scan is outside minimum and maximum thresholds, the Ta values are outside minimum and maximum thresholds (i.e. nonphysical), or the pixel latitude/longitude is out of range, have the appropriate quality flag set and the affected Ta are set to missing.

3.2.5 Cross-track Bias Correction

A falloff in the Ta occurs near the edge of the scan due to obstructions affecting the side lobes of the antenna pattern. The most pronounced decrease is on the right side of the scan, which results in a decrease in the mean observed Ta of several percent or more relative to the center of the scan. An analysis of clear-sky ocean scenes was done for each sensor to determine the magnitude of this falloff. Based on this analysis a scale factor was computed for each pixel position with the center pixel defined as having a multiplier of 1.0. These scale factors are stored in the files `f**_ctbias.dat`. The cross-track biases are subsequently removed from the Ta by dividing each value by the scale

factor correction derived for the given satellite, channel, and pixel position along the scan. These correction coefficients are obtained from the look-up table described in section 3.4.5.3.

3.2.6 Ta to Tb Conversion

Based on a pre-launch analysis of the antenna pattern, described by Colton and Poe (1999), an antenna pattern correction (APC) is applied to the observed Ta to calculate the physical Tb. The Tb is calculated using equation 1, which involves four coefficients for each sensor/channel. This attempts to correct for spillover losses, cross-polarization coupling between channels, and sidelobe contamination. The coefficient C_1 is multiplied by the cross-polarized pixel whereas the coefficient C_2 is multiplied by the previous adjacent pixel Ta and the coefficient C_3 by the next adjacent pixel Ta. The coefficient values are stored in the look-up table described in section 3.4.5.4.

$$Tb_{v,h} = C_0 * Ta_{v,h}(n) + C_1 * Ta_{h,v}(n) + C_2 * Ta_{v,h}(n-1) + C_3 * Ta_{v,h}(n+1) \quad (1)$$

To calculate Tb22v, the above equation requires a Ta22h value, which following Colton and Poe (1999), is obtained by the following:

$$Ta_{22H} = 0.653 Ta_{19H} + 96.6 \quad (2)$$

While the APC coefficients for each of the six SSM/I sensors are provided by Colton and Poe (1999), the decision was made by FNMOC to use the F13 values for F14 and F15 as well for the operational processing of the sensor data record (SDR) files. This was confirmed to be the case by comparing the computed Tb with the SDR Tb values. While detailed information regarding this decision by FNMOC was not available, we chose to be consistent with the SDR record and to account for any residual differences in our subsequent intercalibration analysis.

3.2.7 Intercalibration

F13 was chosen as a calibration standard due to its longevity and stable orbit. The remaining sensors were intercalibrated to F13 using multiple approaches. Five distinct intercalibration techniques were developed. These include direct polar matchups, double differencing against model simulations from reanalysis data, double differencing against matchups with the TRMM Microwave Imager (TMI), vicarious cold calibration and an Amazon warm calibration. Multiple realizations of several of the techniques were applied using different sources of surface and atmospheric geophysical parameters including reanalysis data and retrieval techniques to account for Earth Incidence Angle (EIA) dependent differences between sensors. The purpose of using multiple approaches was 1) because not all approaches were possible for all sensors due to lack of overlap between sensors and with TRMM, 2) to ensure consistency between approaches, 3) to obtain an estimate of the residual calibration uncertainties, and 4) to investigate scene-temperature dependence of sensor calibration differences.

It is important to note that intercalibration does not imply that the resulting Tb will be identical between sensors. Instead, the purpose of the intercalibration is to ensure that measurements between the sensors are “physically” consistent. Physical differences between sensors including diurnal sampling differences and view angle or EIA differences remain and must be accounted for by the geophysical retrieval algorithms.

The derivation of the calibration offsets for each channel of each sensor is described in detail by Sapiano (2013) with additional details in Sapiano et al. (2012). These offsets are stored in the look-up table described in section 3.4.5.5 and used by adding the relevant offset to all data points, which are not the missing data value. Appendix B of Sapiano (2013) shows summary plots of the intercalibration results for pairwise comparison between the SSM/I instruments on different satellites. The F13-F14 comparison is included as Figure 5 below.

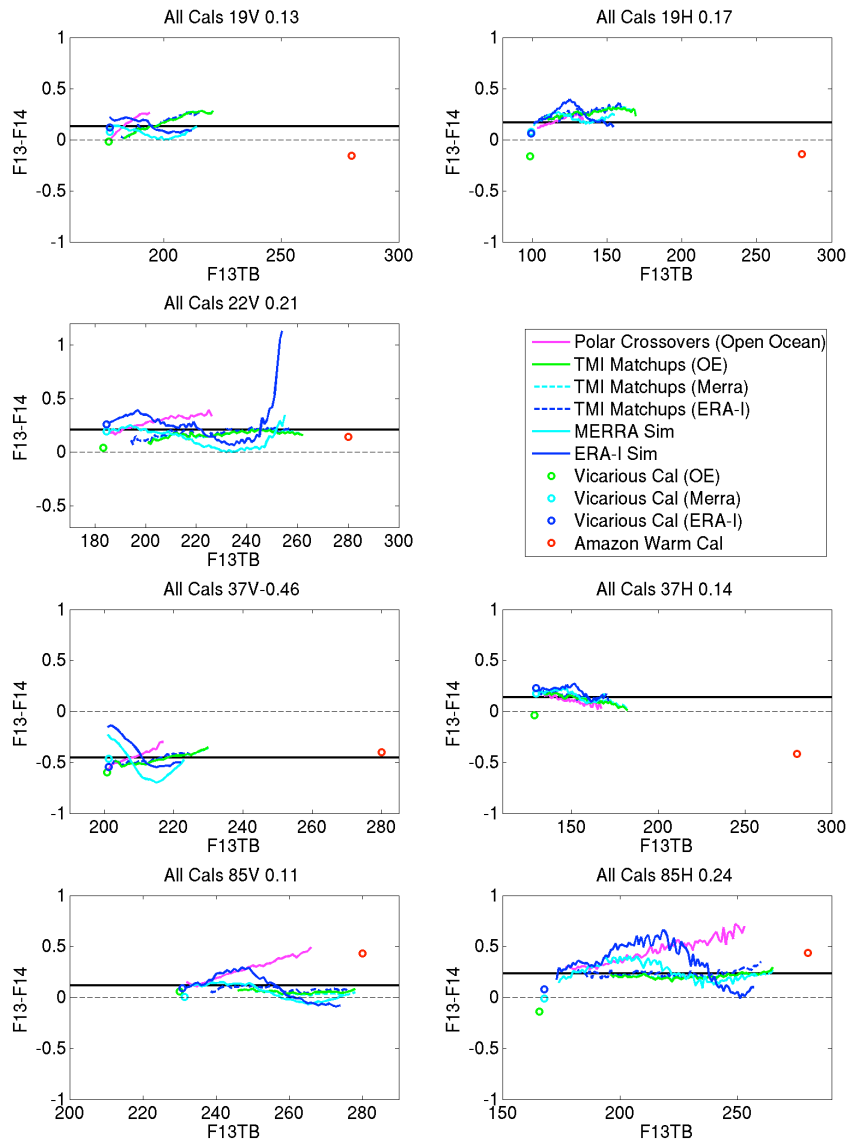


Figure 5: Plots of intercalibration estimates from each implementation by channel for F13 F14.

For the SSM/I sensors simple calibration offsets were used instead of scene-temperature dependent corrections. This was done due to significant uncertainty in the slope or temperature-dependent variations between the various intercalibration approaches, as is evident in Figure 5. With the exception of the Amazon warm cal, which has a larger uncertainty (Sapiro et al. 2013), the other approaches were limited to colder scenes. This lack of reliable information on scene-dependent temperature differences led to the decision to simply apply a Tb offset for each channel.

3.2.8 RADCAL Correction

The activation of RADCAL on F15 in August 2006 caused significant contamination of the TB22V channel. This contamination is removed using an approach similar to that of Remote Sensing Systems described in Hilburn (2009) and Hilburn and Wentz (2008). Our resulting correction is given by the equation

$$Tb22v_{corr} = Tb22v - offset(scan\ position) * factor(hotload) \quad (3)$$

where $Tb22v_{corr}$ is the corrected Tb, $offset(scan\ position)$ and $factor(hotload)$ are obtained from the look-up tables described in section 3.4.5.6. The values stored in these look-up tables were derived by first using a linear regression model to predict Tb22v from the other 6 channels using 2005 data (before RADCAL activation) using non-precipitating ocean scenes (based on the filter developed by Stogryn et al., 1994). The resulting prediction is:

$$\begin{aligned} Tb22v_{pred} = & 0.1444\ Tb19v + 1.1013\ Tb19h + 0.6625\ Tb37v - 1.0975\ Tb37h + \\ & 0.0062\ Tb85v + 0.3245\ Tb85h + 3.5265 \end{aligned} \quad (4)$$

This prediction was found to match the observed data reasonably well. It was then used to predict Tb22v for 2007 data (after RADCAL activation). For each scan position, the mean difference $Tb22v - Tb22v_{pred}$ for 2007 ocean data is the value stored in the look-up table as $offset(scan\ position)$. Simply subtracting this offset from Tb22v results is a reasonable correction for much of the RADCAL-contaminated data, but where the hotload is colder than normal it results in large spikes that indicate a problem with this correction attempt. This is addressed by instead using the multiplicative model defined by 3 as the correction. For 2007 through 2011 data, the values $(Tb22v - Tb22v_{pred}) / offset(scan\ position)$ were calculated, then binned as a function of hotload using 1 Kelvin bins. The mean value of each bin is stored in the look-up table as $factor(hotload)$. A time series of the observed and corrected Tb22v data is shown in Figure 6.

The estimated error in $Tb22v_{corr}$ depends on the hot load temperature, varying from around 3.5 K for values above 290 K to over 5 K when the hot load falls below 270 K. These error estimates show that RADCAL-corrected data is not suitable for climate applications. Hilburn and Wentz (2008) came to the same conclusion that the RADCAL-corrected data may be suitable for many weather applications, but is not of suitable accuracy/stability and therefore should not be used in climate analyses. The quality flag for the low-resolution channels of the RADCAL-corrected Tb22v data (F15

only after August 13, 2006) is set to a value of 13 to indicate that it is unsuitable for climate applications.

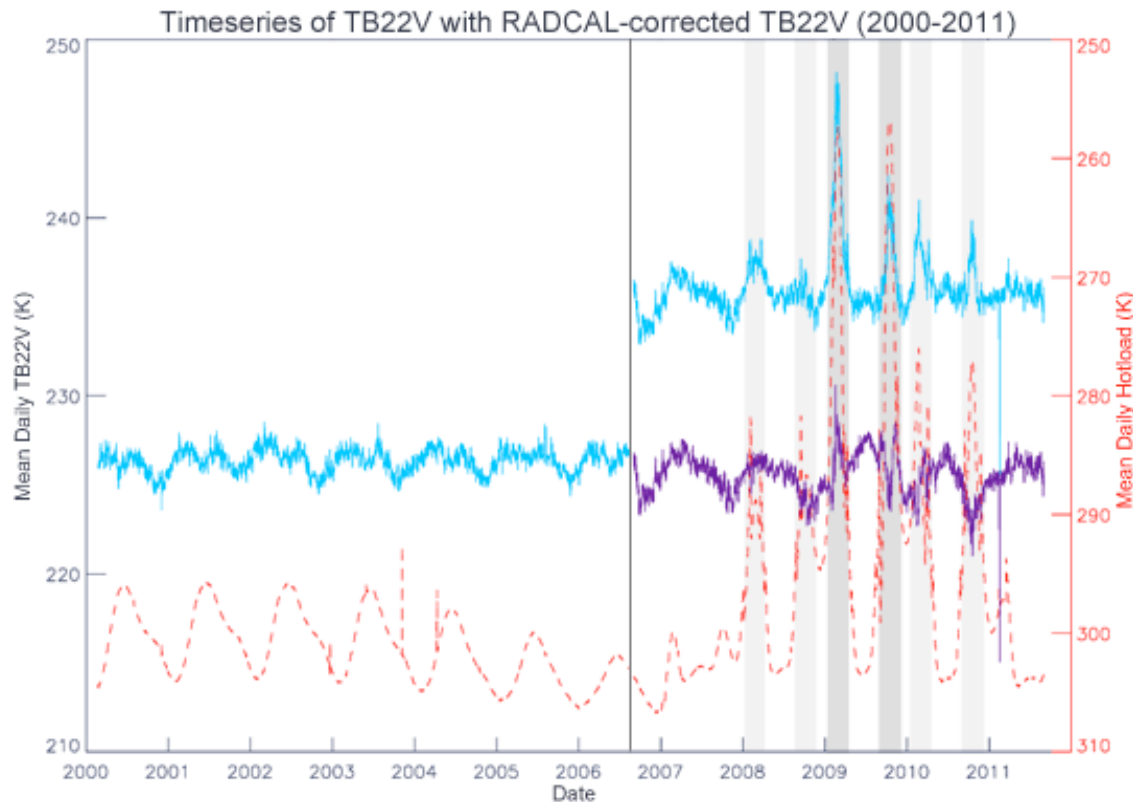


Figure 6: Timeseries of original observed Tb22v (blue) and the RADCAL-corrected Tb22v (purple) based on Equation 3 for ocean scenes between 80S and 80N. The corresponding hot load temperature (dashed red line) is also shown with moderate dips in the hot load temp indicated by the light gray shaded regions and large dips indicated by the dark gray shaded regions. The black vertical line in August of 2006 indicates when the RADCAL beacons were activated.

3.2.9 Write Output

The output FCDR files (described in section 3.4.7) containing the final Tb values with corrections and intercalibration applied are written out in NetCDF4. Note that there is an option in the software to write out an XBASE file, which contains all of the data fields in the input BASE file along with the output FCDR variables and the various satellite/sun angles which are computed but not output in the FCDR file. This option is provided for users wanting to further investigate calibration issues etc.

3.3 Algorithm Input

3.3.1 Primary Sensor Data

The raw sensor data is sensor counts from SSM/I instruments. The sensor counts are converted to antenna temperature (Ta) and stored in the Temperature Data Record (TDR) files created by the Shared Processing Network Data Exchange Format (SPN DEF). These TDR files are subsequently converted into BASE files, which are used as input for the algorithm and are described in section 3.3.3 below.

3.3.2 Ancillary Data (optional)

The Two Line Element (TLE) data created by NORAD containing the satellite orbital elements are used to determine the satellite's position and velocity. The TLE files are in the NORAD TLE format consisting of a title line, which is the satellite name, followed by two lines of formatted text. By default the algorithm uses the precomputed spacecraft position and velocity information stored in the input BASE files.

3.3.3 Derived Data

The input data files used for the FCDR processing are referred to as BASE files. These files contain all of the information from the original source TDR files with the following changes/additions. The BASE files have been reorbitized into single orbit granules with duplicate scans removed and spacecraft position and velocity based on the TLE data added (for later use to calculate geolocation). The BASE files are written in NetCDF4 format with metadata added. With the exception of duplicate scans, none of data from the original TDR files is changed or removed. The idea of the BASE files is to preserve the original data in an easy to read self-describing format and to simplify the subsequent FCDR processing. The format of the BASE files is described in detail in the *SSM/I BASE file Format Specification* (http://rain.atmos.colostate.edu/FCDR/Archive_Docs/formatsspecs/ssmi_base_format_spec_v1.pdf).

3.3.4 Forward Models

No forward models are used in the FCDR processing, however, the development of the intercalibration offsets required radiative transfer calculations to account for differences in EIA between sensors. The models used included the atmospheric absorption model of Rosenkranz (1998), and for ocean surface emissivity, the specular emissivity model based on Deblonde and English (2001) and a rough sea surface model based on Kohn (1995) and Wilheit (1979a,b). More details regarding the implementation of these models is provided in Elsaesser and Kummerow (2008). Only the derived offsets and other coefficients used in the intercalibration and some of the corrections are used in the algorithm.

3.4 Theoretical Description

The software developed for the SSM/I FCDR processing is a stepwise approach described in Section 3.2. This involves reading the input BASE file along with the necessary data coefficient files etc., quality control procedures, calculation of the spacecraft position and velocity (optional) and pixel geolocation, application of cross-track bias corrections, APC correction to compute Tb from Ta, application of intercalibration offsets, and correction for RADCAL interference in the F15 22 GHz channel after August of 2006.

3.4.1 Physical and Mathematical Description

3.4.1.1 Physical Background

Passive microwave sensors, such as the SSM/I, measure the microwave radiation emitted by Earth's surface and atmosphere and interacting with the atmosphere through absorption, scattering, and transmission before reaching the sensor. The amount of absorption and scattering of radiation as it travels through the atmosphere depends on the wavelength (or equivalently, frequency) of the radiation and on the state of the atmosphere (e.g. amount of water vapor, rain, cloud, etc.).

The emission of radiation from Earth's surface and atmosphere is described by Planck's law with the deviation of real materials from ideal blackbodies accounted for by the emissivity (ϵ) of the material. Directly above the surface the brightness temperature (Tb) of a scene at a given frequency is the product of the emissivity of the surface and the scene temperature:

$$Tb = \epsilon T_{actual} \quad (5)$$

The radiation emitted from the surface is subsequently modified by the atmosphere before reaching the satellite sensor, which provides information on the state of the atmosphere. Information about the amount of water vapor, liquid water and ice is inferred from SSM/I data by exploiting known changes in the thermal spectrum due to the absorption, emission, and scattering of radiation. The SSM/I User's Interpretation Guide (Raytheon 2000), section 2, provides theory of remotely sensed electromagnetic radiation – especially microwave radiation – and how it is used to retrieve geophysical atmospheric and surface parameters.

3.4.1.2 Astronomical and Geographical Calculations

The Simplified General Perturbations (SGP4) orbital model (Vallado et al., 2006) is used to calculate perturbations of the satellite orbit due to effects of the sun, moon, Earth's oblateness, etc. The orbital position and velocity of the spacecraft calculated using this model are used along with other satellite and sensor parameters (as described in sections 3.2.3 and 3.4.5.1) to compute the corresponding geolocation or latitude and longitude of each individual pixel or Earth scene.

3.4.1.3 Sensor Characteristics

The physical sensor characteristics and configuration are described in Section 2.2.

3.4.1.4 Simplifications and Approximations

In the quality control processing stage (see section 3.2.4.3), the distance between two pixel locations is approximated by using a sphere to model the Earth.

3.4.2 Data Merging Strategy

The original sampling provided by the six SSM/I sensors is preserved in the output FCDR data with no merging of the resulting data in either space or time. The resulting FCDR Tb from each of the six sensors are intercalibrated to be physically consistent with the observed Tb from F13. Differences between the various sensor Tb due to the local observing time and/or variations in the view angle or EIA remain. Accounting for these differences and merging the data from the various sensors is left to the TCDR developers.

3.4.3 Numerical Strategy

The subroutines to compute the spacecraft position and velocity from the TLE files were implemented based on the North American Aerospace Defense Command (NORAD) SDGP4 code (Vallado et al., 2006). Additional details are provided in the header of the subroutine *sdgp4.c*. Details on the numerical calculations of the pixel geolocation and associated angles are provided in CSU technical report by Sapiano et al. (2012).

3.4.4 Calculations

Details on the processing steps involved in the algorithm are provided in Section 3.2

3.4.5 Look-Up Table Description

Six stages of the algorithm use data that has been calculated and is stored in static look-up tables. The look-up tables used in each stage are described in this section.

3.4.5.1 Calculate Geolocation

The geolocation calculation makes use of the look-up tables contained in the three text files listed below where F** is the satellite designation F08 through F15:

1. geo_SSMI_F**.dat – This file contains data lines which are pairs of a variable name and its value for a variety of time, geometry, sensor alignment, and spacecraft attitude variables.
2. geo_SSMI_F**_rpy.dat – This file contains a line for each month that the satellite was in operation giving values for roll, pitch and yaw.

3. geo_LeapSecs.dat – This file contains a line for each leap second adjustment since 1972 giving values for the Julian day, number of seconds, and sign of adjustment. This data is needed to convert between International Atomic Time (TAI) seconds and Universal Time (UT) seconds.

The geolocation code requires values for satellite and sensor parameters (satellite attitude, sensor alignment, sensor elevation offset and scan angle offset) which are stored in the files geo_SSMI_F*.dat. Published values for the sensor delta elevation angles based on pre-launch measurements are used (Table VI in Colton and Poe, 1999). For scan angle offset, sensor alignment, and satellite attitude, values are determined from the data by the method described in Sapiano and Berg (2012) to correctly locate the boresight.

3.4.5.2 Climatological Quality Check

The mean and standard deviation of the antenna temperatures for each latitude/longitude grid position, each channel, and each month are stored in binary data files named CLIM01.grd for January up to CLIM12.grd for December. The climatological quality check subroutine flags where the fraction of pixels in a scan differing from the mean by more than 3 standard deviations exceeds a threshold.

3.4.5.3 Cross-track Bias Correction

The cross-track bias correction coefficients for each satellite are stored in the binary files F**_cbt_myyy.dat where F** is the satellite name F08 through F15 and myyy is the month that the file was created as the 3-letter month abbreviation and 2-digit year abbreviation (e.g. 'apr12' for April 2012). These files contain the correction coefficients for each scan position for each channel. Cross-track biases are removed from the Ta by dividing each value by the correction coefficient for the satellite, channel, and scan position.

3.4.5.4 Ta to Tb Conversion

The antenna pattern correction (APC) coefficients used to convert Ta to Tb are stored in the text file apc.dat. The derivation of these coefficients is described in Colton and Poe (1999). The coefficients were obtained from Fleet Numerical Meteorology and Oceanography Center (FNMOC) and are from the operational processing code. The APC coefficients obtained from FNMOC are similar to those found in Colton and Poe (1999), Table II (p. 421), columns C0, C1, C2 and C3, but have the following differences:

- The values for satellite F08 channel 85H are different.
- For all satellites and channels, the values of C1, C2 and C3 are negated.
- For satellites F14 and F15, we use the F13 coefficients to be consistent with how the SDR is produced (as explained in an email from Gene Poe with the NRL dated Dec 10, 2004).

3.4.5.5 Intercalibration

The calibration offsets used for intercalibration between the different satellites are stored in the text file `cal.dat`. For each channel of each satellite the delta Tb value to be added to the observed Tb is specified. Since F13 is used as the reference to which the other sensors are calibrated, all of the calibration offsets are zero for the F13 channels.

3.4.5.6 RADCAL Correction

The Tb22v channel of F15 for times after RADCAL activation is corrected using the $Tb22v_{corr} = Tb22v - offset(scan\ position) * factor(hotload)$ (in section 3.2.8 and the quality flag set to indicate that the corrected data is unsuitable for climate applications. This calculation uses two look-up tables stored in the following text files:

1. `radcal_offsets_22v_ocean.dat` – The offset for each low-resolution scan position 1 to 64.
2. `radcal_factors_22v_ocean.dat` – The factors for each 1 Kelvin hot load temperature bin.

3.4.6 Parameterization

The antenna pattern correction or APC is a parameterization of the measured antenna pattern. It is described above in section 3.2.6 and by Colton and Poe (1999).

3.4.7 Algorithm Output

For each input BASE file, the algorithm produces an output FCDR file in NetCDF4 format. There are approximately 15 files per sensor per day and each file is approximately 5.8 Mbytes. Empty files containing only global metadata fields are produced for orbits with no available input TDR data. The FCDR file contains the final intercalibrated Tb for each channel along with pixel latitude and longitude, time for each scan, spacecraft position, quality flags, sun-glint angle, and fractional orbit number with the necessary metadata and supplementary data fields. Two sets of variables are provided. One set corresponds to the five low-resolution channels and the other to the two high-resolution (85 GHz) channels. The data are truncated to the nearest 0.001 degree for the lat/lon values and to the nearest 0.01 K for the Tb and view angles. Internal NetCDF data compression is used to compress the files. A detailed specification of the format of the FCDR files is provided in the *SSM/I FCDR File Format Specification*.

(http://rain.atmos.colostate.edu/FCDR/Archive_Docs/formatsspecs/ssmi_fcdr_format_spec_v1.pdf)

4. Test Datasets and Outputs

4.1 Test Input Datasets

No test datasets were used to characterize the algorithm performance. Validation of the resulting FCDR data is described in Section 5.5.

4.2 Test Output Analysis

4.2.1 Reproducibility

As described in Section 3.2.7 multiple intercalibration approaches were used to check for consistency. Additional details are provided by Sapiano et al. (2012, 2013).

4.2.2 Precision and Accuracy

Since the FCDR are intercalibrated to match the F13 Tb, the accuracy of the values is defined by the accuracy of the F13 Tb. Given the lack of an absolute calibration standard at these frequencies, determination of the absolute accuracy is difficult to determine. Comparison with the CM-SAF and RSS FCDRs as well as comparisons with other independently calibrated sensors including TMI, AMSR-E, WindSat etc. indicate absolute differences less than 2-3 Kelvin. Precision of the results is determined based on consistency between intercalibration approaches (Sapiano et al. 2013) and is generally within 0.5 K for most sensors/channels.

4.2.3 Error Budget

The intercalibration offsets applied in the processing stage described in section 3.2.7 were found as the means over five different techniques, and the standard deviations of the same values provide a measure of the error in the intercalibration. These errors vary from 0.01 K to 0.11 K for the low-resolution channels and from 0.04 K to 0.41 K for the high-resolution channels.

Error Source	Error Magnitude
Sensor Noise	0.6 – 1.1 K
Intercalibration	0.5 K

Table 2: Error Budget

5. Practical Considerations

5.1 Numerical Computation Considerations

This algorithm doesn't use parallelization. No problems with matrix inversions are expected. Failure of the geolocation algorithm to produce a valid latitude and longitude

can lead to missing pixel geolocation in rare instances. There are round-off errors in computations and conversions between different data types, which are expected and within the tolerance of the algorithm.

5.2 Programming and Procedural Considerations

The code implementing this algorithm uses standard procedural programming constructs such as: user-defined data structures to manage input and output data fields; control structures; functions; etc. No unusual programming techniques or optimizations are used as simplicity was an important design criterion. Specific features of the code include:

- A pattern used throughout much of the code is to loop through all the scans of an orbit granule and for each scan to loop through the low-resolution pixels and each low-resolution channel and the high-resolution pixels and each high-resolution channel.
- Each of the seven sequential processing stages of the algorithm can be turned on or off with a flag (these stages are described in section 3.2). This is useful for comparison and validation of individual processing stages, such as comparing the results of our Ta to TB conversion (without intercalibration or any further corrections) with the SDR data set.
- Error and exception conditions are handled by direct checking of conditions/return codes in the main control flow, not by a language-supported exception construct.
- For efficiency (both execution speed and working storage space), extensive use is made of global variables.
- The source code is expected to build, and the resulting program to run, on a considerable range of different platforms. For more information on this, see section 5.6.

5.3 Quality Assessment and Diagnostics

See discussion on Section 5.5 on Validation. This includes application of geophysical retrievals and comparisons with other SSM/I FCDR datasets.

5.4 Exception Handling

Error and exception conditions are handled by direct checking of conditions/return codes in the main control flow rather than by a language-supported exception construct.

5.4.1 Conditions Checked

The following conditions identify errors that necessitate that the program terminate. They are trapped and the program prints a suitable message, then exits gracefully with a non-zero status indicating the type of error.

- If an incorrect number of arguments are supplied to the program, a usage message is printed and it exits with status 1.
- If there is an error opening or reading an input file, the program prints an error message and exits with status 2.
- If there is an error creating or writing to an output file, the program prints an error message and exits with status 2.
- If there are unrecoverable errors in the SGP4 orbital model code, an error message is printed and the program exits with status 5.

The following exceptions are trapped and recovered from by skipping over the item that can't be processed, setting codes to track this, and continuing processing with the next item:

- In the geolocation code, where a vector is expected to intersect the oblate spheroid that models the Earth, the solutions of the equation are checked and if the expected intersection doesn't exist, then the relevant data fields are set to missing and the geolocation is skipped over.

5.4.2 Conditions Not Checked

The following possible error condition is not checked for:

- In the unlikely event that the program would run out of memory, it would crash.

5.4.3 Conditions Not Considered Exceptions

Where data fields are missing or do not satisfy quality control checks (described in section 3.2.4), quality flags are set and for those quality issues classified as serious the corresponding data fields are set to indicate missing data. All corrections/conversions are applied only to non-missing data and if any processing stage identifies certain data as missing, it remains missing for all future processing stages. This is considered normal processing and not an exception condition.

5.5 Algorithm Validation

5.5.1 Validation during Development

Several methods were employed to validate the resulting FCDR data. These included the following.

- 1) Visual inspections and verification of the various corrections applied to the data. For example, as detailed by Berg et al. 2013, to verify the final pixel geolocation, monthly images of gridded ascending minus descending Tb maps were checked using the final roll, pitch, and yaw values for each sensor and compared to maps based on the original TDR data. The results showed consistent improvement over the original data

- 2) Implementation of multiple intercalibration approaches. The use of multiple approaches was done in part to check for consistency between independent calibration techniques. As shown in Figure 5, the resulting differences are generally within 0.5K for all channels. Differences tend to be larger for warm scenes and for the older sensors (F08 and F10), but are generally quite consistent. Scene-dependent differences in the calibration remain an issue to be addressed in the future.
- 3) Comparison with other SSM/I FCDR datasets. To date there are three SSM/I FCDR datasets including the CSU dataset, one produced by Remote Sensing Systems, and one produced by Eumetsat's climate monitoring satellite applications facility (CM-SAF). Comparisons of pixel geolocation and EIA with the CM-SAF show generally good agreement, while there are differences with the RSS results. All three FCDR datasets use different standards for the calibration, with the CSU intercalibrating to F13 and the CM-SAF to F11. RSS appears to use a minimization based on their radiative transfer model and in-situ observations, although this is not completely clear. It should be noted that they have recently released version 7 of their FCDR, however, as of the version 1 release of the CSU FCDR that data was not yet available. We will continue to work with the CM-SAF to compare and validate results and to compare with the RSS version 7 FCDR when it becomes available.
- 4) Application to geophysical retrievals. We are working with several different thematic CDR or TCDR developers to use the CSU FCDR with their algorithms. That effort is ongoing, but since the ultimate measure the FCDR is the consistency of the TCDRs or geophysical retrievals, we will continue to work to solicit feedback from various communities. We have also run two different in house retrieval algorithms to test the consistency of the SSM/I FCDR. Figure 7 shows time series of TPW, ocean wind speed, and cloud liquid water over oceans from the complete SSM/I data record. This retrieval over non-precipitating ocean scenes is based on an optimal estimation approach developed by Elsaesser and Kummerow (2008). While the current implementation of this algorithm is not independently validated as a TCDR, it is a physical retrieval that accounts for changes in EIA between sensors and is very sensitive to calibration differences, making it a useful tool for analyzing the consistency of the FCDR data record. Finally, the latest operational GPROF precipitation retrieval algorithm (Kummerow et al. 2001, 2011) has been applied to the SSM/I FCDR. While these results are not shown here, they are available from (<http://rain.atmos.colostate.edu/RAINMAP>). Both the non-raining and raining time series show some differences, but it is important to remember that the six DMSP spacecraft with SSM/I sensors have different local observing times that drift/decay over time leading to diurnal cycle differences. A comparison of GPROF rainfall estimates based on coincident overpasses with TRMM TMI indicates mean rainfall differences between the SSM/I sensors and with TMI of less than 1%, which is below the mean sampling variability of this metric.

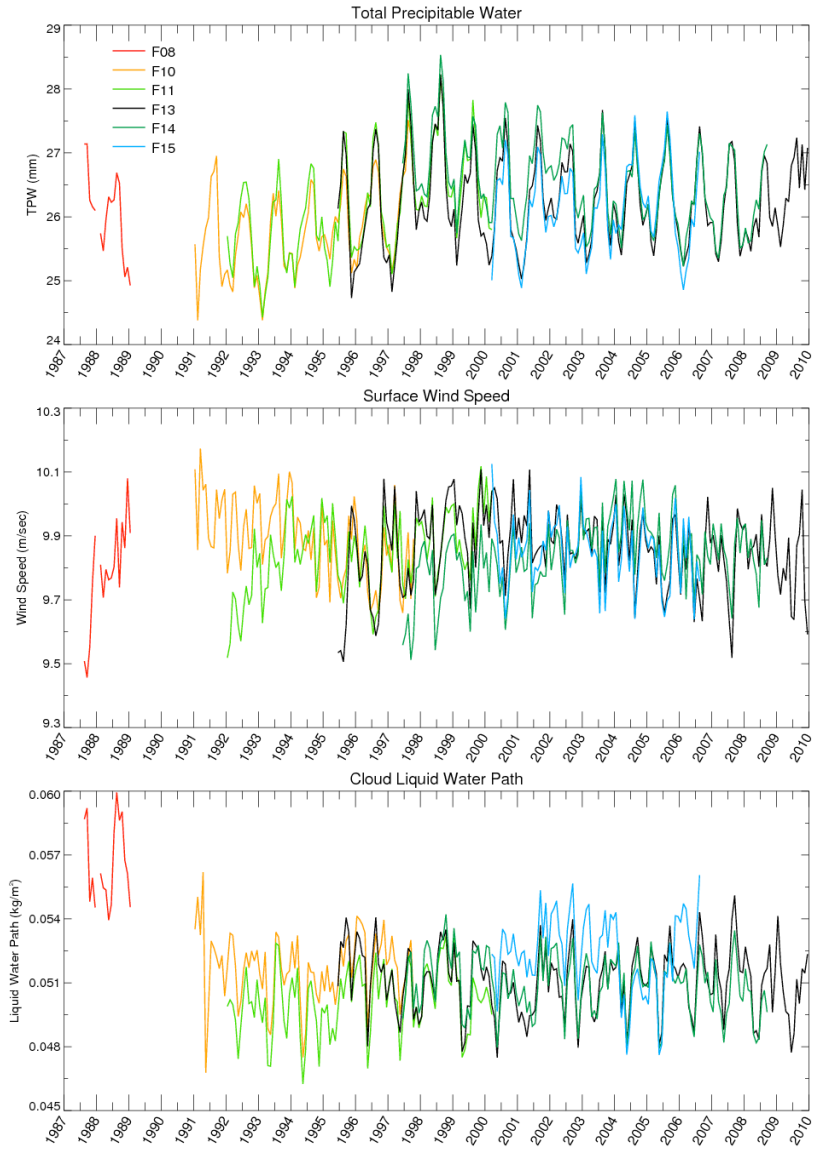


Figure 7: Time series of a) total precipitable water, b) ocean surface wind speed, and c) cloud liquid water path based on the SSM/I FCDR.

5.6 Processing Environment and Resources

The code was originally developed and run in a processing environment described by the features listed in Table 3.

Hardware	Dell PowerEdge R410
Memory	24GB
Processor	Two quad core Intel Xeon CPU X5550 @ 2.67GHz (Hyperthreading enabled so appears as 16 CPUs)

Operating system	CentOS Linux release 5.7 (64-bit)
Programming language	C
Compiler	icc (64-bit)
External libraries	hdf5, netcdf, mfhdf, df, hdf5_hl, jpeg, z, imf

Table 3: Processing Environment

The code has been designed to facilitate running it on different platforms by means of the following methods:

1. The Makefile, which controls the build process, including compiling and linking, contains options to build the system for either 32-bit or 64-bit environments.
2. The code is platform-independent. It was compiled and run using the Intel icc compiler, however, it has also been tested and run using the free gnu gcc compiler.
3. The platform-dependent parts of the code are separated from the rest and found in the file `sgdp4h.h`. This file contains code to:
 - a. Detect the platform;
 - b. For functions that will be used from platform-dependent built-in libraries, load the relevant libraries;
 - c. Handle the precision differences of data types on different platforms.

To build the code in a new environment, follow these steps:

1. Ensure that the required external libraries listed in Table 3 are installed (for hdf, netcdf, jpeg, z, imf).
2. Examine the Makefile and set the compiler command if different for the new environment. Also comment/uncomment lines if necessary to select 32-bit or 64-bit environments.
3. Run the make command to create the executable program `ssmi_fcdr` from the source code.

Performance:

1. Using a single CPU on the system detailed above takes approximately 3 seconds wall clock time to run a single file.
2. Using approximately four processors the entire SSM/I FCDR data record can be reprocessed in less than a week.

3. No temporary storage is required to run the algorithm. The only storage required is for the input and output files. The software with the necessary correction files etc. is less than 200 Mbytes.

6. Assumptions and Limitations

6.1 Algorithm Performance

With the SSM/I sensors, only F15 is still operating and that is in a degraded mode due to the activation of the RADCAL beacons in August 2006 as described in section 3.2.8 and in Milburger and Berg (2012). While the performance of the F15 Tb may degrade over time, as described in this document the resulting RADCAL corrected data is unsuitable for climate applications and should be used with caution.

6.2 Sensor Performance

The sensitivity of the SSM/I instruments is shown in Table 1 and is 0.6 K for the low-resolution channels and 1.1 K for the high-resolution channels. A detailed evaluation of the SSM/I instrument on F08 by Hollinger et al. (1990) also considers gain stability, calibration target stability, spin rate stability, antenna beam characteristics, absolute calibration, and geolocation error and concludes that the F08 SSM/I's sensitivities and stabilities meet or exceed prelaunch performance specifications, except for the degradation and eventual failure of the 85V channel. Colton and Poe (1999) provides an analysis of sensor performance for all SSM/I sensors, which gives similar results as seen for F08.

7. Future Enhancements

Several potential future enhancements have currently been identified. A generic issue for future enhancements is to address any issues identified by users.

7.1.1 Cross-track bias corrections

Revisit the cross-track bias corrections to investigate the potential impact of physical Tb variations across the scan due to roll and pitch variations in the spacecraft attitude.

7.1.2 Warm scene intercalibration

Investigate scene-temperature dependent changes in sensor calibration differences by further developing/investigating warm-scene calibration over the Amazon and/or other warm targets.

7.1.3 Solar and lunar intrusions

Investigate the impact of solar and lunar intrusions into the warm load/cold sky mirror and correct for or flag the affected data.

8. References

Berg, W., C. Kummerow, M. Sapiano, N. Rodriguez-Alvarez, and F. Weng, A Fundamental Climate Data Record of Microwave Brightness Temperature data from 25 Years of SSM/I and SSMIS Observations, *GEWEX Newsletter*, August 2012.

Berg, W. K. and N. Rodriguez-Alvarez, 2013: SSM/I Quality Control, Technical Report, Colorado State University, <http://rain.atmos.colostate.edu/FCDR/>.

Berg, W., M. R. P. Sapiano, J. Horsman, and C. Kummerow, 2013: Improved geolocation and Earth incidence angle information for a fundamental climate data record of the SSM/I sensors, *IEEE Trans. Geosci. Rem. Sens.*, 51, 1504-1513.

Colton, M. C. and Poe, G. A., 1999: Intersensor calibration of DMSP SSM/I's: F-8 to F-14, 1987-1997, *IEEE Trans. Geosci. Rem. Sens.*, 37(1), 418–439.

Deblonde, G., and S. J. English, 2001: Evaluation of the FASTEM-2 fast microwave ocean surface emissivity model. Tech. Proc. Int. TOVS Study Conf. XI, Budapest, Hungary, WMO, 67–78.

Elsaesser, G. S and C. D. Kummerow, 2008: Toward a fully parametric retrieval of the nonraining parameters over the global oceans, *J. Appl. Meteor. Climatol.*, 47, 1599-1618.

Hilburn, K., 2009: Including temperature effects in the F15 RADCAL correction, Technical Report 051209, Remote Sensing Systems, <http://www.remss.com>.

Hilburn, K. A. and Wentz, F. J., 2008: Mitigating the impact of RADCAL beacon contamination on F15 SSM/I ocean retrievals, *Geophys. Res. Lett.*, 35.

Hollinger, J., Lo, R., and Poe, G., 1987: Special Sensor Microwave/Imager User's Guide, Naval Research Laboratory, Washington, D.C.

Hollinger, J. P., Peirce, J. L., and Poe, G. A., 1990: SSM/I Instrument Evaluation, *IEEE Transactions on Geoscience and Remote Sensing*, 28(5), 781–790.

Hollinger, J., 1989: DMSP Special Sensor Microwave/Imager Calibration/Validation, Naval Research Laboratory, Washington, D.C., Vol 1.

Hollinger, J., 1991: DMSP Special Sensor Microwave/Imager Calibration/Validation, Naval Research Laboratory, Washington, D.C., Vol 2.

Kohn, D. J., 1995: Refinement of a semi-empirical model for the microwave emissivity of the sea surface as a function of wind speed. M.S. thesis, Dept. of Meteorology, Texas A&M University, 44 pp.

Kummerow, C. D., S. Ringerud, S. Crook, D. Randel, and W. Berg, 2011: An observationally generated a-priori database for microwave rainfall retrievals, *J. Atmos. Oceanic Technol.*, 28, 113-130.

Kummerow, C. D. and Coauthors, 2001: The Evolution of the Goddard Profiling Algorithm (GPROF) for rainfall estimation from passive microwave sensors. *J. Appl. Meteor.*, 40, 1801–1820.

Milberger, K. and W. Berg, 2012: SSM/I F15 RADCAL Correction for Ocean Data. Technical Report, Colorado State University, <http://rain.atmos.colostate.edu/FCDR/>.

Poe, G. A., Uliana, E., Gardiner, B. and vonRentzell, T., 2006: Mitigation of DMSP F-15 RADCAL Interference with SSM/I, Technical report, NRL, Monterey, CA. Code 7541.

Raytheon Company. Special Sensor Microwave/Imager (SSM/I) User's Interpretation Guide, UG32268-900, Revision C, 29 Nov 2000.

Rosenkranz, P. W., 1998: Water vapor microwave continuum absorption: A comparison of measurements and models. *Radio Sci.*, 33, 919–928.

Sapiano, M. R. P., 2012: Intercalibration of SSM/I and SSMIS for the CSU FCDR. Technical Report, Colorado State University, <http://rain.atmos.colostate.edu/FCDR/>.

Sapiano, M. R. P. and Berg, W., 2012: Estimation of Satellite Attitude for SSM/I and SSMIS Geolocation. Technical Report, Colorado State University, <http://rain.atmos.colostate.edu/FCDR/>.

Sapiano, M. R. P., Berg, W. K., McKague, D. S., and Kummerow, C. D., 2013: Towards an Intercalibrated Fundamental Climate Data Record of the SSM/I Sensors, *IEEE Trans. Geosci. Remote Sens.*, 51, 1492-1503.

Sapiano, M. R. P., Bilanow, S., and Berg, W. K., 2011: SSM/I and SSMIS Stewardship Code Geolocation Algorithm Theoretical Basis. Technical Report, Colorado State University, <http://rain.atmos.colostate.edu/FCDR/>.

Stogryn, A. P., Butler, C. T. and Bartolac, T. J., 1994: Ocean surface wind retrievals from special sensor microwave imager data with neural networks, *J. Geophys. Res.*, 99(C1), 981–984.

Vallado, D. A., Crawford, P., Hujasak, R., and Kelso, T. S., Revisiting Spacetrack Report #3, presented at the AIAA/AAS Astrodynamics Specialist Conference, Keystone, CO, 2006 August 21–24.

Wilheit, T. T., 1979a: A model for the microwave emissivity of the ocean's surface as a function of wind speed. *IEEE Trans. Geosci. Electron.*, 17, 244–249.

Wilheit, T. T., 1979b: The effect of wind on the microwave emission from the ocean's surface at 37 GHz., *J. Geophys. Res.*, 84, 4921-4926.